Light-driven growth in Amazon evergreen forests explained by seasonal variations of vertical canopy structure

Hao Tang[a,1] and Ralph Dubayah[a]

[a]Department of Geographical Sciences, University of Maryland, College Park, MD 20742

Edited by Inez Y. Fung, University of California, Berkeley, CA, and approved January 24, 2017 (received for review October 12, 2016)

Light-regime variability is an important limiting factor constraining tree growth in tropical forests. However, there is considerable debate about whether radiation-induced green-up during the dry season is real, or an apparent artifact of the remote-sensing techniques used to infer seasonal changes in canopy leaf area. Direct and widespread observations of vertical canopy structures that drive radiation regimes have been largely absent. Here we analyze seasonal dynamic patterns between the canopy and understory layers in Amazon evergreen forests using observations of vertical canopy structure from a spaceborne lidar. We discovered that net leaf flushing of the canopy layer mainly occurs in early dry season, and is followed by net abscission in late dry season that coincides with increasing leaf area of the understory layer. Our observations of understory development from lidar either weakly respond to or are not correlated to seasonal variations in precipitation or insolation, but are strongly related to the seasonal structural dynamics of the canopy layer. We hypothesize that understory growth is driven by increased light gaps caused by seasonal variations of the canopy. This light-regime variability that exists in both spatial and temporal domains can better reveal the drought-induced green-up phenomenon, which appears less obvious when treating the Amazon forests as a whole.

Amazon | precipitation | phenology | forest structure | remote sensing

Light is regarded as the main limiting factor for tree growth in tropical rainforests (1–3). High radiation exposure in gaps that result from tree fall in dense canopies can promote the growth of seedlings and juvenile trees, and this regeneration process is characterized by gap dynamic theory (4, 5). Similarly, enhanced light availability during early dry season can increase canopy leaf area and total productivity of canopy and emergent trees, such as the seasonal greening-up phenomenon in Amazon forests (3, 6–8).

However, conflicting observations from field and satellite data challenge the paradigm of light-driven growth. For example, the gap dynamic theory cannot universally explain the advance growth of shade-tolerant trees that dominate tropical forests (5, 9). Most species when facing a tradeoff between high growth rate in large tree-fall gaps and survivorship in shade try to avoid either extreme (5, 10). Adult trees with leaves high in the main and emergent canopy layer have direct access to high radiation loads for increased growth during the dry season. Whether this light-induced greening-up phenomenon in the Amazon is real, or an artifact of passive optical remote-sensing techniques, is still in question (11–15). Multiple studies, from both field surveys and remote-sensing observations, further suggest that water is the main constraint for forest growth during the dry season, and even mild drought can decrease the net carbon uptake with significant leaf abscission and high mortality rates, particularly in the southern Amazon (13, 16–20).

Whereas temporal interactions among herbivory, environmental factors, and forest phenology, and their interannual variability may play a role in determining phenological state, exact mechanisms remain unclear (1, 16, 17). For example, both increased total leaf area and enhanced leaf photosynthetic capacity may possibly contribute to the dry-season greening of the Amazon forests (1, 3, 6–8). Wu et al. (6) suggest increases in capacity occur as old leaves are replaced by new leaves of higher light-use efficiency in the dry season, helping to explain ecosystem photosynthesis dynamics. A further possible explanation is the seasonal dynamics of vertical canopy structure in response to continuous changes of microenvironmental conditions. To explore this issue, we analyzed seasonal leaf area index (LAI) dynamics of both canopy and understory over intact Amazon forests using data from the Geosciences Laser Altimeter System (GLAS), onboard NASA's Ice, Cloud and land Elevation Satellite (ICESat) (21). Lidar-based observations provide direct and accurate measurements of leaf area density for both the canopy and understory layer in tropical forests (22, 23), and can also characterize multitemporal canopy structure dynamics (24). Additionally, lidar does not suffer from potentially confounding artifacts in passive optical satellite images, e.g., resulting from variations in sun-sensor geometry (11, 12, 14). We first mapped seasonal LAI changes of canopy and understory across three acquisition periods mainly in March, June, and October, respectively (Fig. S1). Next, we examined relationships between LAI changes and seasonal variations of two climatic variables, precipitation and solar radiation, over the Amazon as a whole, and within four different climate zones identified from monthly precipitation data (Fig. S2). Finally, we quantified observed differences between canopy and understory LAI seasonally and investigated their potential interaction.

Results

Canopy LAI exhibited significant seasonal variations (Fig. 1 *A*–*C*, Table 1, and Fig. S3), the spatial pattern of which coincided

Significance

Observations of field experiments and satellite imagery have led to a significant debate about light-driven growth of Amazon forests during the dry season. We help resolve these conflicts using observations from spaceborne lidar, and show that both canopy and understory have an opportunistic ecological response to the radiation and moisture regimes. Our research is placed within a consistent ecological framework that links gap theory, field-based studies, and the remote-sensing data record, and which illuminates mechanistic responses of the understory and canopy forming trees to changes in light and water.

Author contributions: H.T. and R.D. designed research; H.T. performed research; H.T. and R.D. analyzed data; and H.T. and R.D. wrote the paper.

The authors declare no conflict of interest.

This article is a PNAS Direct Submission.

[1]To whom correspondence should be addressed. Email: htang@umd.edu.

This article contains supporting information online at www.pnas.org/lookup/suppl/doi:10.1073/pnas.1616943114/-/DCSupplemental.

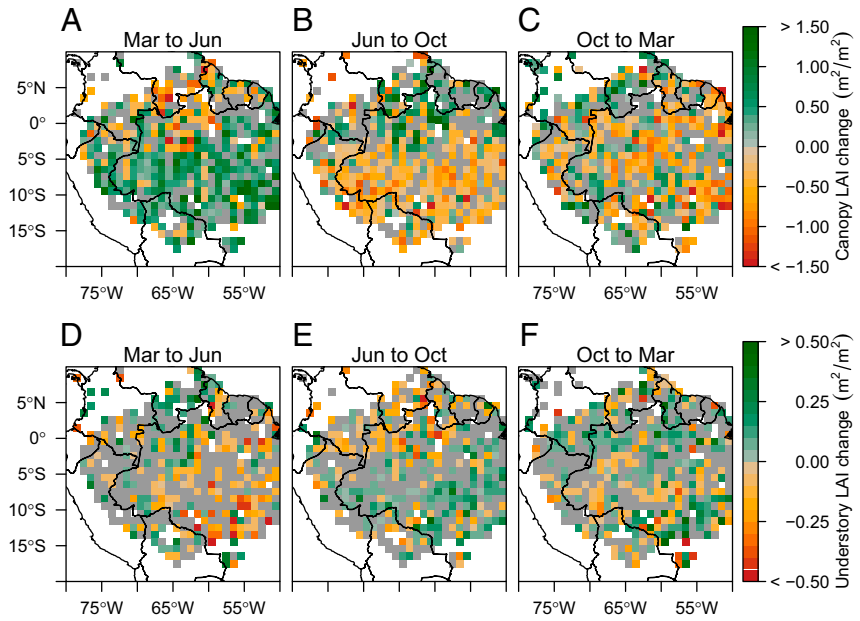

Fig. 1. Seasonal changes in canopy LAI and understory LAI over the Amazon. Each 1° pixel represents the mean canopy LAI change (*A–C*) or understory LAI change (*D–F*) for three GLAS acquisition periods: March to June, June to October, and October to March (of the following year), using data pooled from 2003 to 2006. In all cases, the LAI change is expressed as the later period minus the earlier one. Spatial distribution of canopy greening-up coincides with the approximate start of dry season but in an asynchronous mode (*A–C*), as different parts of Amazon have different starting months of the dry season (Table 1 and Fig. S2). The understory also shows a seasonal cycle (*D–F*) but with an opposite variation to canopy. Note the different scale bars between canopy and understory. Gray pixels represent areas where the observed mean LAI change is less than standard error for that cell (*Materials and Methods*).

with the seasonal drifting of precipitation (Fig. S2) for all zones other than the western Amazon. Increases in canopy LAI (i.e., green-up) corresponded with the start of the dry season as it generally progressed from south to north. The pattern started in the southern Amazon from April to June and shifted toward the central Amazon from July to October, ending in the north from December toward March of the next year. However, the substantial gain of canopy foliage did not sustain throughout the entire dry season (the duration of dry season may exceed 6 months and overlap two GLAS acquisition periods). For the southern Amazon, the greening of canopy in the early dry season (from March to June; Fig. 1*A*) was largely offset by loss of LAI (i.e., browning) in the mid to late dry season (from June to October; Table 1, Fig. 1*B*, and Fig. S4). During the wet season, most Amazon forests showed either no significant change, or a slight decrease in canopy LAI with a magnitude much smaller than the late dry season (Table 1, Figs. S3 and S4).

Magnitude of the canopy greening in the dry season was greater in the southern forests ($\Delta LAI = 0.38$ m^2/m^2 from March to June, ~8% of the total canopy LAI value) than the rest of Amazon ($\Delta LAI = 0.22$ m^2/m^2 in central forests from June to October, and $\Delta LAI = 0.19$ m^2/m^2 in northern forests from October to March) (Table 1 and Fig. S4). The western Amazon forests did not show any significant change in canopy LAI across the three observation periods. When aggregated over all four climate zones, the canopy LAI changes for the Amazon as a whole were $\Delta LAI = 0.22$, −0.10 and −0.11 m^2/m^2 for all three periods, respectively (Fig. S5).

Table 1. Seasonal variation of forest structural variables at four different climate zones in Amazon

Climate zones[†]	Dry season duration	Forest structure layers[‡]	Annual mean LAI, m²/m²	LAI change[§], m²/m²		
				Mar to Jun	Jun to Oct	Oct to Mar
Southern Amazon	May to Oct	Canopy	4.52	***0.38****	**-0.27***	**−0.11***
		Understory	0.61	***−0.03****	**0.03***	0.00
Central Amazon	Jul to Dec	Canopy	4.57	0.03	***0.22****	**−0.24***
		Understory	0.56	−0.02	*-0.02*	**0.03***
Northern Amazon	Nov to Apr	Canopy	3.76	−0.13	−0.05	***0.19****
		Understory	0.82	**0.07***	**−0.08***	*0.00*
Western Amazon	No dry season	Canopy	4.67	−0.01	0.07	−0.06
		Understory	0.48	0.00	**−0.03***	**0.03***

[†]Climate zones were created based on dry and wet season timing using monthly aggregated precipitation data from the TRMM (*Materials and Methods* and Fig. S2). The wet-to-dry season transition progresses seasonally from south to north (with the approximate seasonal start set in italics in Table 1), except for the western Amazon, which has no pronounced dry season compared with the other regions (17).

[‡]A height threshold of 10 m was used to separate understory from the canopy layer, and the understory defined here does not distinguish among young regenerating trees and lower canopy (Fig. S7).

[§]Canopy and understory LAI changes in individual climate zones were estimated from aggregations of corresponding 1° cells (*$P < 0.05$; the change observed is different from 0 in bold). The LAI change is expressed as the later period minus the earlier one (e.g., June − March).

The understory also exhibited a seasonal variation of LAI, but mostly in an opposing temporal pattern compared with the canopy layer (Fig. 1 *D*–*F*, Table 1, and Figs. S3 and S6), decreasing during the start of dry season. Increases in understory LAI mainly occurred in the middle or end of dry season when the shedding of canopy leaves was largely completed, as inferred by the negative changes in canopy LAI. The increases could also happen at the end of wet season but before the start of dry season (e.g., around 10°S, 55°W in Fig. 1*F*). Although the magnitude of understory LAI changes was small (Fig. S7), its relative change rate (i.e., percentage change to its annual mean) exceeded 50% for individual cells (Fig. S8).

Significant relationships were observed between shifts in canopy LAI and climatic variables, similar to previous studies (8, 11). Seasonal changes in canopy LAI showed a negative correlation with changes in precipitation (r^2 = 0.17, 0.15, and 0.05, respectively, for the three periods with all P <0.01), and a slightly weaker positive correlation with variations of solar radiation (r^2 = 0.08, 0.03, and 0.03, respectively, with all P < 0.01; Fig. S9). However, only a weak ($r^2 \leq 0.05$) or insignificant relationship ($P >$ 0.05) was found when relating understory LAI changes with either precipitation or radiation (Fig. S10). In contrast, increases in understory LAI had strong negative correlations with the decrease of canopy LAI for all three periods (Fig. 2 and Fig. S10).

Discussion

The spatial pattern of lidar-derived canopy LAI dynamics shows an increase of ~5–8% during the wet-to-dry season transition, although the magnitude of observed changes varied geographically, with a maximum in the southern Amazon (Table 1 and Fig. S3). These results support the hypothesis of dry season green-up within Amazon forests reported in previous studies (3, 6–8, 11, 14, 19). Our changes are largely consistent with results from Wu et al. and Guan et al. (6, 19), which reported increases varying from ~5–10% using Moderate Resolution Imaging Spectroradiometer (MODIS) enhanced vegetation index (EVI).

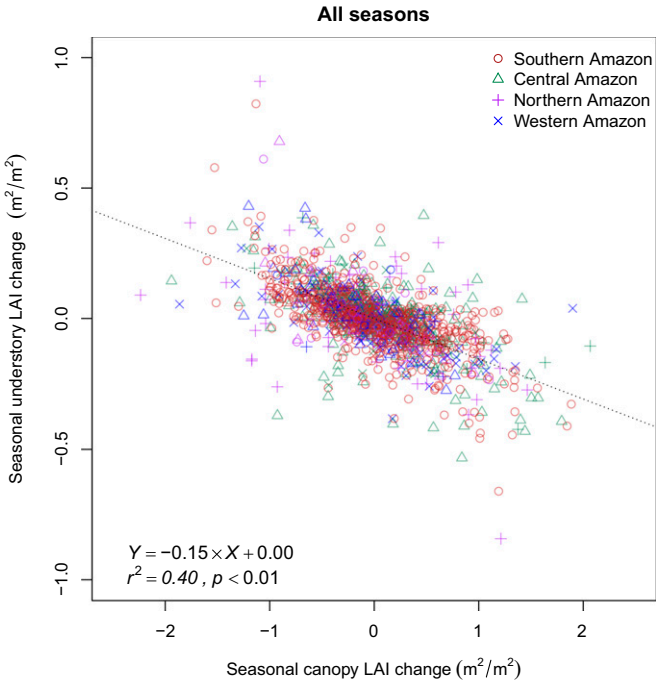

Fig. 2. Relationship between seasonal understory and canopy LAI changes across Amazon forests. Strong and consistent negative correlations are found across all climate zones throughout the seasonal cycle (dashed line generated from an ordinary least-squares model), suggesting the abscission of crown structure plays a fundamental role on understory development across Amazon forests (Fig. S11).

Our analyses also reveal that seasonal change of canopy phenology corresponds with the spatial and temporal change of precipitation (Fig. 1 and Fig. S9). These results support field studies that leaf flushing coincides with the increased light exposure at the early stage of the dry season (3, 6). The loss of LAI of canopy leaves (Fig. 1 *A*–*C*) during the middle or late dry season highlights the importance of water availability on leaf development as well, and supports the hypothesis that mild drought potentially may have a negative impact on forest growth when plant water deficits exceed critical thresholds (15, 17, 19). Such is the example in the southern Amazon, where we observed a significant loss of canopy foliage during its 6-month dry season. We note that a similar lidar study over Amazon forests did not see these dynamics (12), because it used limited ICESat data from only one period (June and October), thus missing the pervasive spatial temporal variations in canopy and understory LAI present in the complete record.

The greening of understory at late dry season and its opposing seasonal variation with the canopy layer reveal a potential interaction between canopy and understory in the Amazon. We did not observe this interaction in dry forests outside the basin area where water is the main limiting factor (Fig. S8). These results are consistent with previous findings that, in tropical rainforests, the growth of light-limited understory plants has a strong phenological preference for maximal irradiance conditions when the canopy layer is deciduous during the dry season (1, 25). Our results also suggest that crown structural dynamics and associated changes in microenvironment on understory development may contribute a stronger influence than seasonal climatic variability in precipitation and radiation (2, 4, 26). One potential explanatory mechanism may be that understory plants do not benefit from the increased insolation (i.e., top of canopy solar radiation) during the early dry season because most of it is intercepted by new canopy leaves with high light-use efficiency. Subsequently, understory plants and small trees grow with increased canopy gap openings either in the midlate dry season (after canopy abscission) or at the end of wet season (but before canopy flushing). Previous studies in dense tropical forests suggest that even a decrease of 5% in dry-season LAI can enhance the light reaching the forest floor by more than 50% relative to the wet season, although the absolute radiation level may still remain as low as 1% (27, 28). Meanwhile, strong evapotranspiration from largely intact canopy allows the understory to maintain low water deficits by moistening the air at boundary layer (29). The favorable microenvironment, combined from light and water conditions, therefore promotes the growth of understory in the late dry season as indicated by the increase of understory LAI in the Amazon.

This seasonal gap-creation growth hypothesis provides a complementary explanation for the growth of shade-tolerant and slow-growing trees in tropical rainforests. It suggests that enhanced subcanopy radiation transmission caused by seasonal variations of the canopy layer (e.g., from sun flecks or enhanced diffuse light) may play a critical role in tropical forest regeneration in addition to large tree-fall gaps (5, 9, 28). This is consistent with the strategy taken by tropical dry semideciduous forests, where partial crown cover may optimize seed germination and seedling establishment, balancing light requirements and water limitations (26, 30). Most tropical forests are essentially semideciduous with abscission levels varying along moisture gradients (1, 30).

Our results further suggest that Amazon forests may optimize phenological processes with an anticipatory response to reliable environmental factors (1), such as regular seasonality. The large-scale LAI dynamics we observed with lidar agrees with the conceptual leaf turnover hypothesis and field studies that trees maximize the carbon gain by flushing new leaves of high photosynthetic capacity at the end of the wet season, and reduce the respiratory loss by dropping old leaves before water stress during the dry season (1, 6, 27, 28, 30). Further examination of these

processes will require a more thorough and precise characterization of vertical canopy structure at finer temporal and spatial scales, potentially available from terrestrial and airborne lidar, as well as future spaceborne lidar missions (31).

Materials and Methods

ICESat-GLAS Lidar Analysis. The GLAS instrument on board ICESat is a 1,064-nm full-waveform lidar sensor widely used for measuring vertical forest structure and aboveground biomass. It records forest structural information by sampling the Earth's surface in transects using footprints at ~65-m-diameter footprints (32). The along-track distance between footprints is 175 m and the between-track distance is about 30 km at the Equator. Vertical LAI distribution can be derived from the waveform based on a Geometric Optical and Radiative Transfer model (22, 33, 34). The performance of the lidar-LAI model has been validated over several sites that represent major forest types around the world (22, 23, 35–37). In the model, we used a seasonally averaged reflectance ratio (i.e., leaf reflectance/litter reflectance) of 1.03 to rule out the possibility of reflectance-driven increases in LAI during the dry season [reflectance data were adopted from a previous study (12); Table S1]. We did not consider the variation of clumping conditions within the canopy, and thus calculated effective LAI only (not true LAI) consistent with radiation-interception-based indirect measurements, such as from LAI-2000 instruments, hemispherical photos, and most remote-sensing techniques (38, 39). We did not use the waveform centroid relative height (WCRH) applied in a previous lidar study (12), because WCRH is not a direct measurement of canopy cover but an approximation, primarily designed to assess the surface roughness of Shuttle Radar Topography Mission (SRTM) data (40).

We used a GLAS dataset reprocessed from the standard GLA14 lidar data over Amazon forests from laser operation campaigns between 2003 and 2006. The campaigns covered the Amazon area over three periods: late February to March, late May to June, and early October to November (Fig. S1). The reprocessed GLAS data separated the recorded laser signal between ground and vegetation with up to six Gaussian fits (Fig. S1), eliminated most spurious observations, and were largely free from cloud contamination, signal saturation, or slope effects (41). Specifically, we applied the following thresholds to select high-quality GLAS footprints: (*i*) SRTM slope <10°; (*ii*) amplitude of the ground Gaussian fit >0.05 (volt), and (*iii*) area of the ground Gaussian fit >1 (volt × nanosecond). We also excluded the entire L2c campaign from analysis because its low laser power could fail to penetrate through dense canopy (Table S2). The remaining nine laser campaigns largely captured seasonal variation conditions across different parts of the Amazon (Fig. S1). Both a wetland/inundation map (42) and an MODIS land cover map (43) were applied to select footprints over evergreen broadleaf forests only. We also excluded nonforest footprints from further analysis based on the International Geosphere-Biosphere Programme (IGBP) forest definition (44): canopy height greater than 5 m and total fractional cover greater than 0.3. This resulted in 919,492 footprint level measurements of LAI that were then averaged within each 1° cell with a minimum footprint number requirement of 40 for each seasonal GLAS acquisition period (Figs. S1 and S2). Finally, seasonal mean LAI changes in canopy and understory were calculated among the three periods (the later period minus the earlier one). To examine if there was any sampling bias at 1° cell resolution, we also analyzed temporal LAI dynamics of canopy and understory by averaging ICESat footprints in a given observation campaign over climate zones (*Climate Data Analysis*) (Fig. S3).

Sensitivity Analysis of GLAS LAI. We assessed the measurement error of GLAS by comparing the derived LAI data set with high-quality airborne lidar data acquired from NASA's Laser Vegetation Imaging Sensor (LVIS) (45). We could not quantify such error directly from comparisons of ground measurements because there was no spatially overlapping field survey available during the GLAS acquisition periods. We estimated the total measurement error by propagating LVIS measurement error to GLAS footprint level as follows:

The measurement error of LAI profile from individual LVIS shot showed no significant bias and had a $\sigma_{LVIS} = 1.36$ m^2/m^2 in comparison with destructively sampled field data in a tropical rainforest (22). The standard error of the mean (SEM) of LVIS LAI measurement averaged over a GLAS footprint were thus quantified as

$$\sigma_{avg\_LVIS} = \sigma_{LVIS} \Big/ \sqrt{N_{LVIS}}, \quad [1]$$

where N_{LVIS} is the number of LVIS shots falling within a GLAS footprint. Here we aimed to minimize the LVIS sampling error by choosing $N_{LVIS} > 13$ (approximately the area ratio between GLAS and LVIS footprint), and estimated the σ_{avg_LVIS} to be <0.36 m^2/m^2. We reanalyzed spatially overlapping GLAS and LVIS data sets with a minimum $N_{LVIS} > 13$ at different sites across the conterminous United States (36). We screened out GLAS footprints of no distinct canopy layer (with the maximum canopy height <15 m) and those having a slope value >10°. The comparisons between GLAS and LVIS had an $r^2 = 0.82$, *bias* = −0.21, *RMSE* = 0.68 m^2/m^2 and residual standard error (*RSE*) = 0.65 m^2/m^2 for total LAI, and an $r^2 = 0.50$, *bias* = 0.01, *RMSE* = 0.38 m^2/m^2 and *RSE* = 0.38 m^2/m^2 for understory LAI (0~10 m in height). We calculated the footprint level measurement error (σ_{GLAS}) of total LAI and understory LAI to be 0.75 and 0.52 m^2/m^2, respectively, by propagating all error terms as

$$\sigma_{GLAS} = \sqrt{\sigma^2_{avg\_LVIS} + RSE^2_{GLAS\_LVIS}}. \quad [2]$$

The SEM for GLAS LAI values at 1° cells (σ_{avg_GLAS}) were estimated to be <0.12 and 0.08 m^2/m^2 for canopy and understory, respectively. They were calculated as

$$\sigma_{avg\_GLAS} = \sigma_{GLAS} \Big/ \sqrt{N_{GLAS}}, \quad [3]$$

where N_{GLAS} is the number of GLAS footprints within a given cell [the minimum N_{GLAS} is 40 (Fig. S1)]. The standard error for the mean LAI difference in a cell was then found as a function of the sample variances and σ_{avg_GLAS}. Cells with seasonal mean LAI difference less than this standard error were masked gray in Fig. 1.

Climate Data Analysis. We analyzed impacts of two climatic variables, precipitation and solar radiation, on seasonal changes of lidar observed canopy and understory LAI. Monthly quarter-degree precipitation data from Tropical Rainfall Measuring Mission (TRMM Product 3B43) were averaged to 1° between 1997 and 2015 (46). The maximum values of monthly mean 1° radiation data were obtained from Clouds and the Earth's Radiant Energy System (CERES Product EBAF-Surface_Ed2.8) between March 2000 and June 2015 (47). We calculated the normal monthly conditions by averaging multiyear measurements. Seasonal changes in precipitation and radiation were then calculated among the three lidar operation periods (Fig. S1).

We followed the dry season definition used in a previous study (8) with months having precipitation <100 mm or less than one-third the annual precipitation range. Pixels with monthly minimum precipitation >150 mm were classified as areas with no seasonality. The climate zones were classified according to the starting time of dry season: April to June in the south, July to September at the center, and October to March in the north (Fig. S2), and showed similar spatial variations of dry season in Amazon forests identified by previous studies (17, 48). We applied regression analysis between changes of climate data and LAI over the entire Amazon area for all seasons (Fig. 2), as well as for each individual period (Figs. S9 and S10).

ACKNOWLEDGMENTS. We thank S. Los for technical help with raw ICESat-GLAS data processing; and M. Zhao for technical help with TRMM and CERES data analysis (archived at https://trmm.gsfc.nasa.gov/ and https://ceres.larc.nasa.gov//). We are also grateful to J. Armston, S. Hancock, L. Duncanson, and S. McMahon for insightful comments. The ICESat-GLAS data are archived at https://nsidc.org. Funding for this research was provided by NASA Global Ecosystem Dynamics Investigation mission (Grant NNL15AA03C).

1. Wright SJ, Vanschaik CP (1994) Light and the phenology of tropical trees. *Am Nat* 143(1):192–199.
2. Chazdon RL, Pearcy RW (1991) The importance of sunflecks for forest understory plants - photosynthetic machinery appears adapted to brief, unpredictable periods of radiation. *Bioscience* 41(11):760–766.
3. Saleska SR, et al. (2003) Carbon in Amazon forests: Unexpected seasonal fluxes and disturbance-induced losses. *Science* 302(5650):1554–1557.
4. Denslow JS (1987) Tropical rain-forest gaps and tree species-diversity. *Annu Rev Ecol Syst* 18:431–451.
5. Wright SJ, et al. (2010) Functional traits and the growth-mortality trade-off in tropical trees. *Ecology* 91(12):3664–3674.
6. Wu J, et al. (2016) Leaf development and demography explain photosynthetic seasonality in Amazon evergreen forests. *Science* 351(6276):972–976.
7. Huete AR, et al. (2006) Amazon rainforests green-up with sunlight in dry season. *Geophys Res Lett* 33(6):L06405.
8. Myneni RB, et al. (2007) Large seasonal swings in leaf area of Amazon rainforests. *Proc Natl Acad Sci USA* 104(12):4820–4823.
9. Brown ND, Whitmore TC (1992) Do dipterocarp seedlings really partition tropical rain-forest gaps. *Philos Trans R Soc London Ser B-Biological Sci* 335(1275):369–378.
10. Lieberman M, Lieberman D, Peralta R (1989) Forests are not just Swiss cheese - Canopy stereogeometry of non-gaps in tropical forests. *Ecology* 70(3):550–552.

11. Hilker T, et al. (2014) Vegetation dynamics and rainfall sensitivity of the Amazon. *Proc Natl Acad Sci USA* 111(45):16041–16046.
12. Morton DC, et al. (2014) Amazon forests maintain consistent canopy structure and greenness during the dry season. *Nature* 506(7487):221–224.
13. Saleska SR, et al. (2016) Dry-season greening of Amazon forests. *Nature* 531(7594): E4–E5.
14. Bi J, et al. (2015) Sunlight mediated seasonality in canopy structure and photosynthetic activity of Amazonian rainforests. *Environ Res Lett* 10(6):64014.
15. Jones MO, Kimball JS, Nemani RR (2014) Asynchronous Amazon forest canopy phenology indicates adaptation to both water and light availability. *Environ Res Lett* 9(12):124021.
16. Lewis SL, Brando PM, Phillips OL, van der Heijden GMF, Nepstad D (2011) The 2010 Amazon drought. *Science* 331(6017):554.
17. Brando PM, et al. (2010) Seasonal and interannual variability of climate and vegetation indices across the Amazon. *Proc Natl Acad Sci USA* 107(33):14685–14690.
18. Davidson EA, et al. (2012) The Amazon basin in transition. *Nature* 481(7381):321–328.
19. Guan KY, et al. (2015) Photosynthetic seasonality of global tropical forests constrained by hydroclimate. *Nat Geosci* 8(4):284–289.
20. Asner GP, Alencar A (2010) Drought impacts on the Amazon forest: The remote sensing perspective. *New Phytol* 187(3):569–578.
21. Schutz BE, Zwally HJ, Shuman CA, Hancock D, DiMarzio JP (2005) Overview of the ICESat Mission. *Geophys Res Lett* 32(21):L21S01.
22. Tang H, et al. (2012) Retrieval of vertical LAI profiles over tropical rain forests using waveform lidar at La Selva, Costa Rica. *Remote Sens Environ* 124:242–250.
23. Stark SC, et al. (2012) Amazon forest carbon dynamics predicted by profiles of canopy leaf area and light environment. *Ecol Lett* 15(12):1406–1414.
24. Dubayah RO, et al. (2010) Estimation of tropical forest height and biomass dynamics using lidar remote sensing at La Selva, Costa Rica. *J Geophys Res* 115:G00E09.
25. Engelbrecht BMJ, et al. (2007) Drought sensitivity shapes species distribution patterns in tropical forests. *Nature* 447(7140):80–82.
26. Vieira DLM, Scariot A (2006) Principles of natural regeneration of tropical dry forests for restoration. *Restor Ecol* 14(1):11–20.
27. Parker G, Tinoco-Ojanguren C, Martinez-Yrizar A, Maass M (2005) Seasonal balance and vertical pattern of photosynthetically active radiation within canopies of a tropical dry deciduous forest ecosystem in Mexico. *J Trop Ecol* 21:283–295.
28. Wirth R, Weber B, Ryel RJ (2001) Spatial and temporal variability of canopy structure in a tropical moist forest. *Acta Oecologica-International J Ecol* 22(5–6):235–244.
29. Juarez RIN, Hodnett MG, Fu R, Goulden ML, von Randow C (2007) Control of dry season evapotranspiration over the Amazonian forest as inferred from observations at a southern Amazon forest site. *J Clim* 20(12):2827–2839.
30. Murphy PG, Lugo AE (1986) Ecology of tropical dry forest. *Annu Rev Ecol Syst* 17: 67–88.
31. Dubayah R, et al. (2014) The Global Ecosystem Dynamics Investigation. *American Geophysical Union, Fall Meeting 2014* (AGU, San Francisco).
32. Abshire JB, et al. (2005) Geoscience Laser Altimeter System (GLAS) on the ICESat Mission: On-orbit measurement performance. *Geophys Res Lett* 32(21):L21S02.
33. Ni-Meister W, Jupp DLB, Dubayah R (2001) Modeling lidar waveforms in heterogeneous and discrete canopies. *IEEE Trans Geosci Remote Sens* 39(9):1943–1958.
34. Harding D (2001) Laser altimeter canopy height profiles: Methods and validation for closed-canopy, broadleaf forests. *Remote Sens Environ* 76(3):283–297.
35. Tang H, et al. (2014) Deriving and validating Leaf Area Index (LAI) at multiple spatial scales through lidar remote sensing: A case study in Sierra National Forest, CA. *Remote Sens Environ* 143:131–141.
36. Tang H, et al. (2016) Characterizing leaf area index (LAI) and vertical foliage profile (VFP) over the United States. *Biogeosciences* 13(1):239–252.
37. Armston J, et al. (2013) Direct retrieval of canopy gap probability using airborne waveform lidar. *Remote Sens Environ* 134:24–38.
38. Chen JM, Cihlar J (1995) Plant canopy gap-size analysis theory for improving optical measurements of leaf-area index. *Appl Opt* 34(27):6211–6222.
39. Chen J, Menges C, Leblanc S (2005) Global mapping of foliage clumping index using multi-angular satellite data. *Remote Sens Environ* 97(4):447–457.
40. Carabajal CC, Harding DJ (2006) SRTM C-band and ICESat laser altimetry elevation comparisons as a function of tree cover and relief. *Photogramm Eng Remote Sensing* 72(3):287–298.
41. Los SO, et al. (2012) Vegetation height and cover fraction between 60° S and 60° N from ICESat GLAS data. *Geosci Model Dev* 5(2):413–432.
42. Hess LL, et al. (2015) Wetlands of the Lowland Amazon Basin: Extent, vegetative cover, and dual-season inundated area as mapped with JERS-1 Synthetic Aperture Radar. *Wetlands* 35(4):745–756.
43. Friedl MA, et al. (2010) MODIS Collection 5 global land cover: Algorithm refinements and characterization of new datasets. *Remote Sens Environ* 114(1):168–182.
44. Belward AS (1996) *The IGBP-DIS Global 1 km Land Cover Data Set "DISCover": Proposal and Implementation Plans* (IGBP-DIS Office, Toulouse, France).
45. Blair JB, Rabine DL, Hofton MA (1999) The Laser Vegetation Imaging Sensor : A medium-altitude, digitization-only, airborne laser altimeter for mapping vegetation and topography. *ISPRS J Photogramm Remote Sens* 54(2–3):115–122.
46. Huffman GJ, Stocker EF, Bolvin DT, Nelkin EJ, Adler RF (2012) TRMM Version 7 3B42 and 3B43 Data Sets.
47. Kato S (2015) CERES Level 3 EBAF-Surface Terra+Aqua netCDF File - Edition 2.8, 10.5067/Terra+Aqua/CERES/EBAF-Surface_L3B.002.8.
48. Xiao X, Hagen S, Zhang Q, Keller M, Moore B (2006) Detecting leaf phenology of seasonally moist tropical forests in South America with multi-temporal MODIS images. *Remote Sens Environ* 103(4):465–473.